Evaluating sources of surface bias in HRRR using New York State Mesonet

Lanxi Min[1], David R. Fitzjarrald[1], Yuyi Du[1], Brian E. J. Rose[2], Jia Hong[1,3] and Qilong Min[1]

[1]Atmospheric Sciences Research Center, University at Albany, Albany, New York, USA.

[2]Department of Atmospheric and Environmental Sciences, University at Albany, Albany, New York, USA.

[3]State Key Laboratory of Information Engineering in Surveying, Mapping and Remote Sensing, Wuhan University, Wuhan, Hubei, China.

Corresponding author: Qilong Min (qmin@albany.edu)

Key Points:

- The HRRR model surface thermodynamic biases are seasonally dependent, presenting a systematic warm and dry bias during the warm season.
- The primary locations of the summer warm and dry biases are over farmland, on days with optically thick clouds.
- A hydrological bias underestimating of spring snow melt is consistent with subsequent summer warm and dry biases over farmland.

Abstract

In recent years, there has been increasing demand for applications of shortterm forecasting of renewable energy potential and assessments of the likelihood of extreme weather events using the High-Resolution Rapid Refresh (HRRR) model. Examining the biases in the newest version of HRRR is necessary to promote further model development. Using data from the most comprehensive and dense monitoring network, New York State Mesonet (NYSM), we evaluated HRRR version 3 meteorological fields for an entire year. In this work, the land-atmosphere-cloud coupling system is evaluated as an integrated whole. We investigated the physical processes influencing the soil hydrological balance and the thermodynamic interactions, from surface fluxes up to the level of boundary layer convection from both temporal (seasonal and diurnal) and spatial perspectives. Results show that the model 2m temperature and humidity biases are seasonally dependent, with warm and dry bias present during the warm season, and an extreme nocturnal cold bias in winter. The summer warm bias includes both a land-surface-induced bias and a cloud-induced bias. Inacurate representation of energy partition and soil hydrological process across different land use types and hydrological bias of spring snow melt in the land surface model is identified as the main source of the land-surface induced bias. A feedback loop linking cloud presence, radiative flux changes and temperature contributes to the cloud-induced bias. The positive solar radiation bias increases from clear sky to overcast sky conditions. The most significant bias occurs during overcast and thick cloud conditions associated with frontal passage and thunderstorms.

1 Introduction

Understanding land-atmosphere coupling is essential for improving weather forecasts at multiple scales (Betts et al., 2013). Soil and vegetation influence the partition of surface energy fluxes, which in turn affecting planetary boundary layer (PBL) development, convective initiation, cloud development, and precipitation (Pleim et al., 2011; Smirnova et al., 2016; Sun et al., 2017; Lee et al., 2018). Subsequent cloud formation and precipitation modulate the exchange of radiation, heat, and moisture in the boundary layer, a feedback that alters surface thermodynamic conditions (Stull, 1988; Fitzjarrald et al., 2001; Freedman et al., 2001; Betts & Silva Dias, 2010). This complex, nonlinear feedback process has been the topic of numerous simulation and observational studies dealing with the land atmosphere interaction (e.g., Eltahir et al., 1998; Schar et al., 1999; Koster et al., 2004; Koster et al., 2006; Taylor et al., 2012; Williams et al., 2016; Peters et al., 2017). Williams et al. (2016) evaluated the single-column version of Community Land Model (CLM4.5) using observations in the U.S. Southern Great Plains. They found the model underpredicted evaporative fraction and overpredicted the impact of soil moisture, leading to biases in the 2-m air temperature and precipitation. Peters et al. (2017) analyzed the impact of surface moisture on the forecasting of a mesoscale convective system (MCS), finding that the initial onset and subsequent MCS displacement was strongly correlated with the model bias in near-surface humidity.

The HRRR (High-Resolution Rapid Refresh) model was developed to serve the US severe weather and aviation forecasting community by providing frequently updated high-resolution short-range weather forecasts (Benjamin et al., 2016). HRRR is highly flexible, and has been used to develop many valuable forecast applications, including more accurate predictions of thunderstorms and flooding potential (Bytheway et al., 2017; Katona et al., 2016;

Griffin et al., 2017), air quality (James et al., 2018), and renewable energy forecasting (Pichugina et al., 2017; James et al., 2017). The performance of HRRR forecasts in terms of land-atmosphere interaction has been evaluated in previous works (Wagner et al., 2019; Lee et al., 2019). Wagner et al. (2019) evaluated HRRR diurnal variation of convective available potential energy (CAPE) against CAPE obtained from surface-based Atmospheric Emitted Radiance Interferometer (AERI) measurements, finding that HRRR-forecasted CAPE lagged 2 to 4 hours compared to the observations. This is believed to result from the lack of subgrid-scale clouds in version 1 of the HRRR. Lee et al. (2019) also evaluated the HRRR forecasted near-surface meteorological fields and surface energy balance using measurements from two micrometeorological sites. They found that although HRRR-forecasted near-surface temperature and moisture are in good agreement with observations, there are notable positive biases in sensible heat flux, biases that might lead to modeled precipitation underestimates.

The complex landscape of New York State and its immediate surroundings offer a unique opportunity to study the effects of aerosol-cloud-precipitation interactions on weather systems in complex terrain that rely on strong land-atmosphere coupling . In response to increasingly frequent extreme weather events, the University at Albany, SUNY (UAlbany) developed an Early Warning Severe Weather Detection network. This unique network measurement suite, known as the New York State Mesonet (NYSM), fills a critical need of providing data for in-depth model evaluation. It is well-suited for NWP model evaluations of mesoscale processes and comparison with the NYSM observations forms the basis of this study to evaluate HRRR model performance. Our goal in this study is to identify the spatial and temporal error structure and sources of surface thermodynamic variables, and investitgate its link to land surface, atmosphere and cloud coupling processes. Furthermore, we aim to indentify processes that are candidates for inclusion during future model improvement.

2 Data and Methods

2.1 HRRR

HRRR v3 model is based on WRF-ARW v3.8.1. It was developed by NOAA, with 3-km resolution, hourly updated, cloud-resolving, convection-allowing atmospheric model. The model region covers the whole Continental United States (CONUS). The scalar grid dimensions are 1799 × 1059. Since the operational version of the HRRR (currently HRRRv3) was implemented on 12 July 2018, we will perform one-year evaluation between September 1, 2018 and August 31, 2019. In the HRRRv3, 15-sec land use information and 30-sec Leaf Area Index from Moderate Resolution Imaging Spectroradiometer (MODIS) was used as initial condition. The Rapid Update Cycle (RUC) land surface model is used to compute surface heat flux and moisture exchanges (Smirnova et al., 2016). The surface skin temperature is calculated using surface energy balance, itself controlled by the shortwave and longwave radiation budget, and the energy partition of sensible and latent heat fluxes. A two-layer snow model was used in RUC. Snow can be melted from the top and bottom of snowpack. Bottom layer melted water infiltrates into soil, and tops layer goes into surface runoff (Smirnova et al. 2016). A frozen soil physics algorithm is used in RUC to take into account freezing and thawing processes in soil. In this algorithm, direct effect of energy releases in soil water changing phases and the change of thermal conductivity of the soil column is considered (Smirnova et al. 2000). HRRR v3 used the Thompson microphysics scheme with five hydrometeor types (cloud water, cloud ice, rain, snow and graupel) which improved the upper level cloud biases in comparison to the previous version

(Thompson & Eidhammer, 2014). To better represent sub-grid scale shallow-cumulus clouds, the MYNN Planetary Boundary Layer Scheme is used, with assumed sub-grid cloud probability distribution functions to determine the subgrid scale cloud mixing ratio, cloud fraction, and the buoyancy flux (Olson et al., 2019). The Rapid Radiative Transfer Model for GCMs (RRTM-G) is used to estimate radiative forcing (Iacono et al., 2008). This study focuses on the short-term (1 - 24 hours) forecast from 0 UTC analyses.

2.2 New York State Mesonet (NYSM)

The diverse topography and mosaic of land cover types characteristic of New York State elicit a strong challenge to models aiming to describe the impact of land surface/atmosphere interactions on forecast quality. Large coverage of deciduous forest introduces strong seasonality on land surface conditions, which in turn strongly modulate the surface energy partition, itself partially controlling boundary layer development. Interleaved with forest are other important surface types, such as forest, farmland and urban landscapes. This mosaic challenges the model's ability to represent the transition zones that separate land surface types. Complex terrain effects such as valley-induced LLJs and channeling of the winds is important for the break of stability at the early morning, which further complicates the cloud formation processes (Freedman et al., 2001; Freedman and Fitzjarrald, 2017). All of these characteristics provide a good testbed for understanding the processes of land atmosphere-cloud coupling.

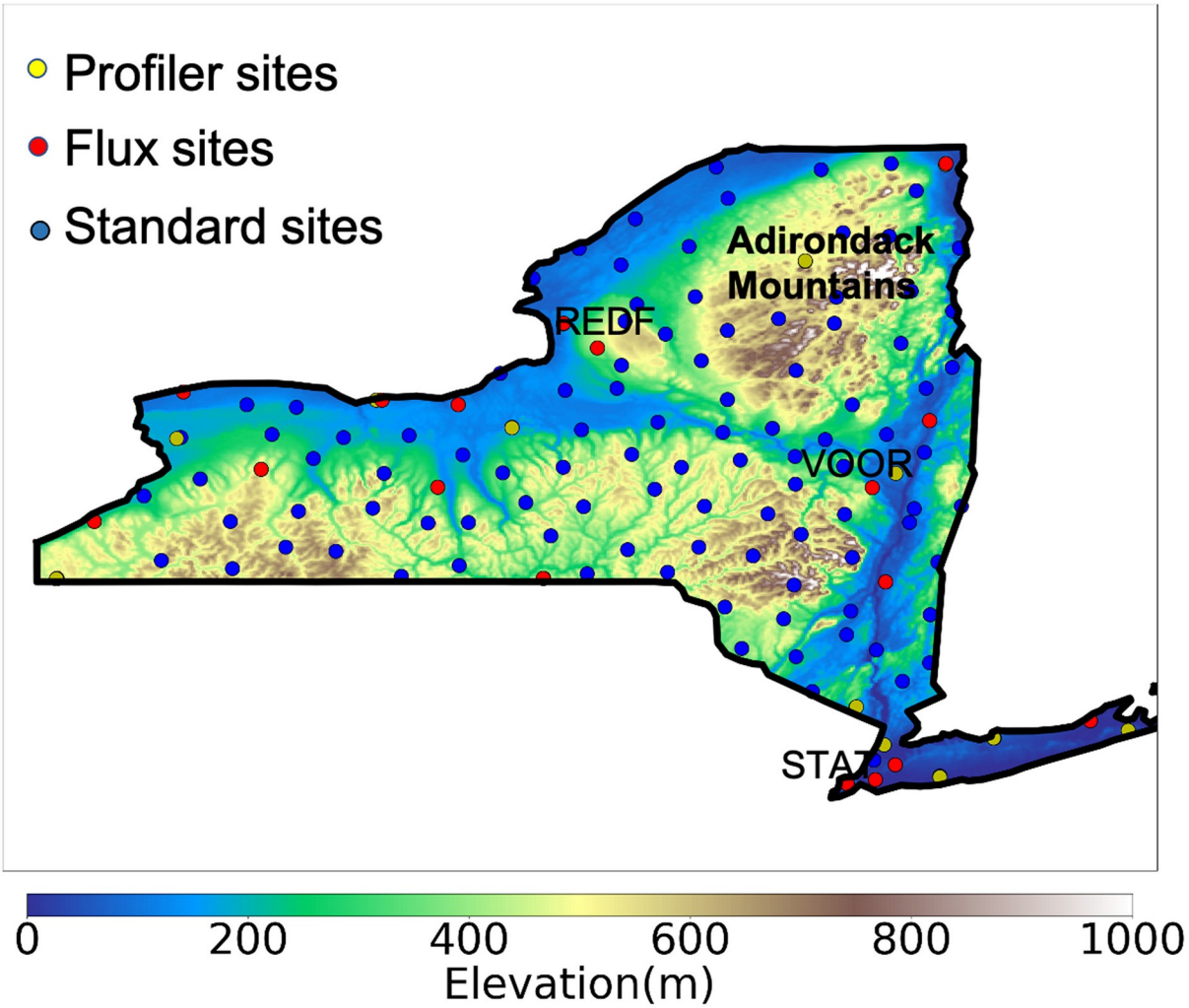

Figure 1. Topography of THE research area identifying the 17 profiler sites, 17 flux sites and 126 standard stations of the New York State Mesonet. Redfield (REDF) is a typical forest site. Voorheesville (VOOR) is an orchard (farmland and forest mosaic) site. Staten Island (STAT) is an urban site. The Adirondack mountains are primarily covered by deciduous forest.

In 2017, UAlbany deployed and began operating a dense environmental monitoring network, New York State Mesonet (NYSM, http://nysmesonet.org/). The 180-site NYSM has operated with state-of-the-art instrumentations, including 126 standard surface meteorology stations, 17 flux towers and 17 atmosphere profilers, currently the most sophisticated, high density (average distance between stations ~ 26 km) statewide observing network (see Figure 1). The 126 standard surface stations measure not only standard meteorological variables (temperature, humidity, wind speed and direction, pressure, and precipitation) but also soil temperature and moisture at three levels, snow depth, and total surface short-wave (SW) irradiance at 5-minute intervals (Brotzge et al., 2020). The sub-network of 17 enhanced surface energy budget stations directly measure both incoming and outgoing shortwave and longwave radiation, ground heat flux, and turbulent fluxes of momentum, sensible and latent heat, and carbon dioxide with 30 minutes intervals. The locations of 17 flux sites were selected to represent New York State land surface types, including farmland, forest, urban and etc.

Topograghy is also considered to avoid obstruction proximity (Covert, 2019). To be comparable to HRRR, only data sampled at an hourly interval are used in this paper.

As NWP models transit to a high-resolution convection-allowing framework, infrequent atmospheric sounding profiles (currently only 2 soundings per day at three sites within New York State) are inadequate. Recognizing this critical measurement gap, the NYSM operates 17 enhanced atmospheric profiler systems that are sited along population, transportation and utility corridors, strategically positioned to capture upwind features approaching the station (Freedman et al., 2016). Each profiler site is equipped with a wind Doppler LiDAR (WDL), a profiling (multi-frequency) microwave radiometer (MWRP) and the environmental Sky Imager-Radiometer (eSIR). The profiler network continuously samples the vertical profiles of temperature, humidity with MWRP from surface to 10 km (Yang & Min, 2018). MWRP significantly increased temporal resolution of temperature and humidity vertical measurements. Compensated with higher vertical resolution from soundings, MWRP measurements can lead to better understanding of boundary layer conditions. eSIR is a dual-measurement system comprised of continuous (daytime) observations of aerosol and cloud optical depths, narrowband spectral direct and diffuse radiation, and whole sky images (cloud distribution and motion for solar energy forecasting). The WDL provides not only 3D wind fields (up to 7 km) but also planetary boundary layer (PBL) height and vertical profile of aerosol optical properties (synergistic with eSIR inferred aerosol optical depth). The multi-frequency MWRP independent information on temperature and moisture, and cloud liquid water--crucial data for determining upper atmospheric conditions (Yang & Min, 2018) and cloud optical properties (Min & Harrison, 1996). This advanced instrument suite provides an unprecedented data stream of aerosols, clouds, radiation, precipitation, multi-level soil moisture/temperature, snow depth/snow water content, surface fluxes, and meteorological profile data at high spatial and temporal resolution, providing the ability to track abrupt changes in thermodynamic profiles throughout the state.

To quantify the cloud conditions at the standard sites where eSIR is not available, the observed global horizontal irradiance (GHI) or total solar radiation was used to calculate the clear-sky index (CSI). The clear-sky index is the ratio of observed GHI to the baseline GHI under clear-sky conditions in that month. A simple clear sky model was used to calculate clear-sky solar radiation (Robledo & Soler, 2000):

$$GHI = A \times (\cos z)^{B} \times \exp\left(C \times \left(90^{0} - z\right)\right) \qquad (1)$$

Where GHI is the Global Horizontal Irradiance; z is solar zenith angle; and A, B, C are the fitting parameters at specific site, derived from GHI measurements on selected clear-sky days in one month. Consequently, the CSI describes the atmospheric clear-sky or cloudy-sky conditions, defined as

$$CSI = \frac{GHI}{GH\,I_{clear-sky}} \qquad (2)$$

Specifically, we classified the weather conditions as:

- Clear-sky conditions with CSI > 0.8.

- Transition conditions with CSI between (0.6, 0.8), in which either optically thin clouds or broken clouds are present in the sky.

- Overcast conditions with CSI <= 0.6.

3 Results

3.1 Temporal and spatial analysis of the HRRR 2-m forecast

The 2-m temperature and relative humidity are key meteorological parameters for diagnosing and evaluating model performance. They are strongly influenced by the coupling processes between land and atmosphere. During the warm season there are consistently warm and dry biases during both daytime and nighttime (Figure 2). The daytime maximum temperature bias, however, is anti-correlated with the bias of the nocturnal minimum temperature ($r \approx -0.49$). This suggests that low-level cloud dynamics might play an important direct role in elucidating the diurnal cycle of the warm season surface temperature bias. During the daytime, low-level clouds tend to block the shortwave radiation and cool the surface. However, at night, the same low-level clouds reduce the outgoing longwave radiation and keep the surface warm. An inaccurate representation of low-level clouds during both daytime and nighttime is a possible reason for the negative correlation. In contrast, both biases of maximum and minimum temperatures during the cold season show no significant average systematic biases, with extreme negative biases on the coldest days. The daytime maximum temperature bias and nocturnal minimum temperature bias are positive correlated ($r \approx 0.36$), indicating potentially distinct physical processes other than low cloud bias controlled the cold season surface biases. In winter, the snow freezing and melting processes largely modulate the surface temperature and humidity. The freezing and thawing processes in the snow cover and soil are possibly responsible for the cold extreme biases (Viterbo et al., 1999; Garc´ıa-D´ıez et al., 2013)

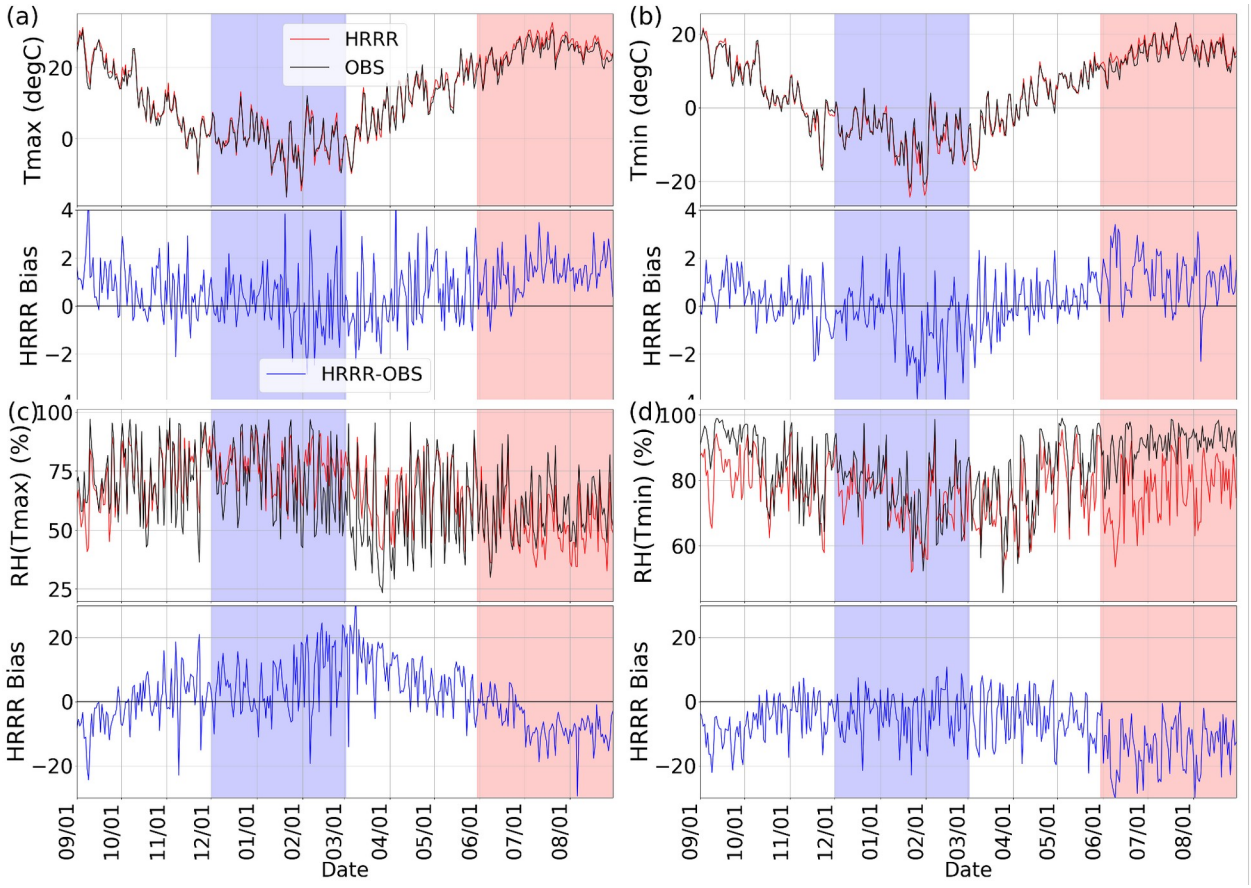

Figure 2. Average time series of data from 126 NYMN sites and simulation results from HRRR: (a) daily maximum temperature and (b) is daily minimum temperature; (c) corresponding relative humidity to daily maximum temperature. and (d) corresponding relative humidity to daily minimum temperature. The blue shaded area is the cold season and the red shaded area is the warm season.

The HRRR vegetation module incorporates monthly updated MODIS (Moderate Resolution Imaging Spectroradiometer) satellite retrieved vegetation. In New York, the transition seasons (spring, fall) rapidly progress northward in spring or retreat to the south in fall (Fitzjarrald et al., 2001). Significant changes in vegetation "greenness", soil temperature, and soil moisture in a few weeks during leaf emergence coincide with corresponding changes in the surface energy partition. Figure 2 also shows these distinct seasonal transitions in the 2-m temperature and RH bias characteristics that occurred around mid-May (during spring onset and leaf emergence) as well as mid-October (during leaf senescence in New York State), indicating that the HRRR model physics associated with the spring and fall season transition may lack precision. Detailed statistics of daily maximum/minimum temperature and relative humidity for each month are listed in Table 1. These strong seasonality of biases in temperature and RH suggests that there are potential issues with the land-atmosphere coupling in the HRRR.

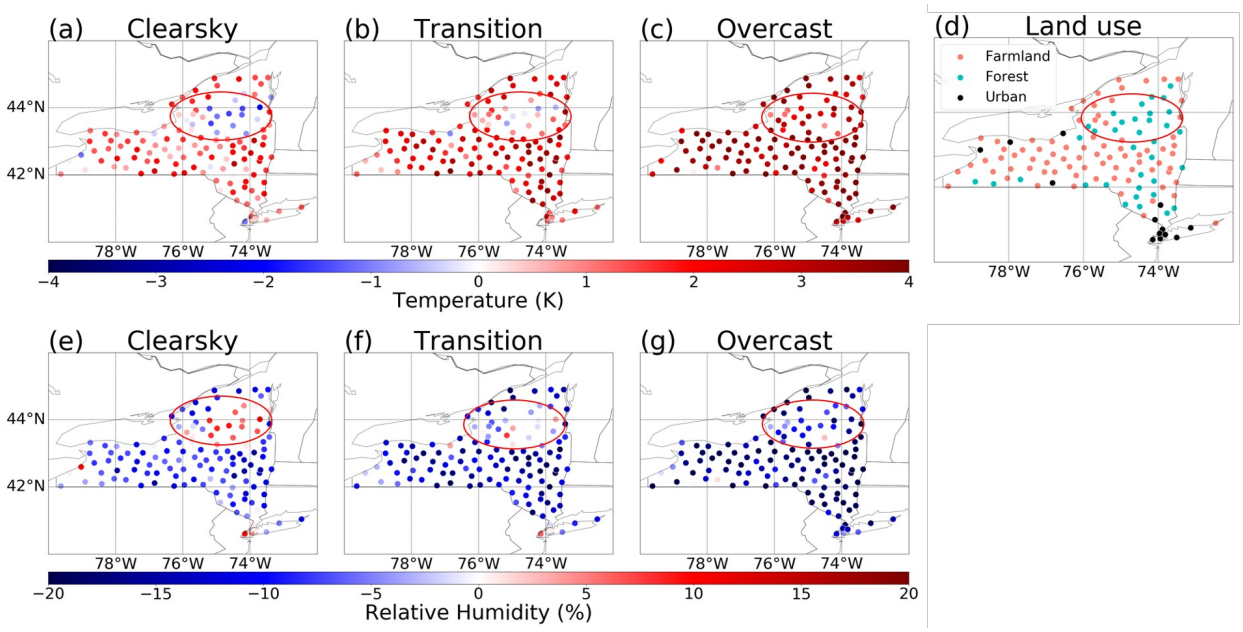

Figure 3. Spatial distribution of the 2-m temperature and RH biases classified by clear sky index in July 2019 over NYSM 126 standard sites: (a) and (e) clear-sky conditions with CSI > 0.8; (b) and (f) transition conditions with CSI between (0.6, 0.8); and (c) and (g) overcast conditions with clear sky index <= 0.6. (hour 0900-1700). The red circle indicate the Adirondack region.

Table 1. Mean Bias Error (MBE), Root Mean Square Error (RMSE) of daily maximum/minimum temperature, relative humidity between 126 standard NYSM sites and the HRRR over period 1 Sep. 2018 to 31 Aug. 2019. Statistics are based on all hourly observations and averaged over monthly and separated by different land use types (farmland and forest). Tmax is the daily maximum temperature; Tmin is the daily minmum temperature; Hmax is the relative humidity when temperature is maximum; Hmin is the relative humidiy when temperature is minimum.

	Farmland				Forest			
	Tmax (MBE)	Tmax (RMSE)	Hmax (MBE)	Hmax (RMSE)	Tmax (MBE)	Tmax (RMSE)	Hmax (MBE)	Hmax (RMSE)
Jan	0.17	1.25	2.96	7.62	0.25	1.26	3.06	6.65
Feb	-0.13	1.7	10.56	10.24	-0.07	1.67	11.45	11.41
Mar	-0.23	1.21	13.91	7.95	-0.69	1.27	17.82	10.63
Apr	0.82	1.4	4.1	9.16	0.05	1.6	12.32	9.08
May	0.92	0.87	-2.15	4.68	0.1	1.12	3.45	6.09
Jun	0.94	0.87	-2.15	4.68	0.1	1.12	3.45	6.09
Jul	1.94	0.72	-11.23	3.4	1.07	0.93	-5.69	5.54
Aug	1.64	0.69	-10.55	5.34	1.17	0.8	-7.46	5.8
Sep	1.24	1.03	-7.72	5.88	1.02	0.98	-5.11	6
Oct	0.57	0.97	0.68	5.54	0.67	1.1	-0.12	7.82
Nov	0.32	1.02	3.17	8.41	0.67	1.1	0.7	11.18
Dec	0.24	0.79	3.12	6.03	0.28	0.7	1.42	7.86

The dense NYSM network enables us to study the HRRR performance, as a function of heterogeneous land covers, and soil conditions under a variety of weather conditions. In the warmest month, (July, 2019), the spatial patterns of 2-m temperature and humidity biases are correlated closely to the land surface types under all weather conditions (Figures 3a-3d). The forest sites, particularly at Adirondack northern plateau forest regions, have lower or even opposite 2-m temperature biases compared to the nearby farmland sites under all weather conditions. Table 1 also shows that in warm season (June, July, August), the mean 2-m temperature biases are much larger over farmland. The dependence of land use type further illustrates a potential issue in the Rapid Update Cycle (RUC) Land Surface Model (LSM) used by the HRRR. Figure 3 also shows the cloud control on surface warm biases. We found that the most significant bias comes during conditions with cloud overcast. It is hypothesized that land surface energy partition and cloud forcing are two main factors controlling the warm season surface temperature bias. We will discuss this hypothesis further in section 3.3 and section 3.4 below.

3.2 Soil hydrological process in land surface model

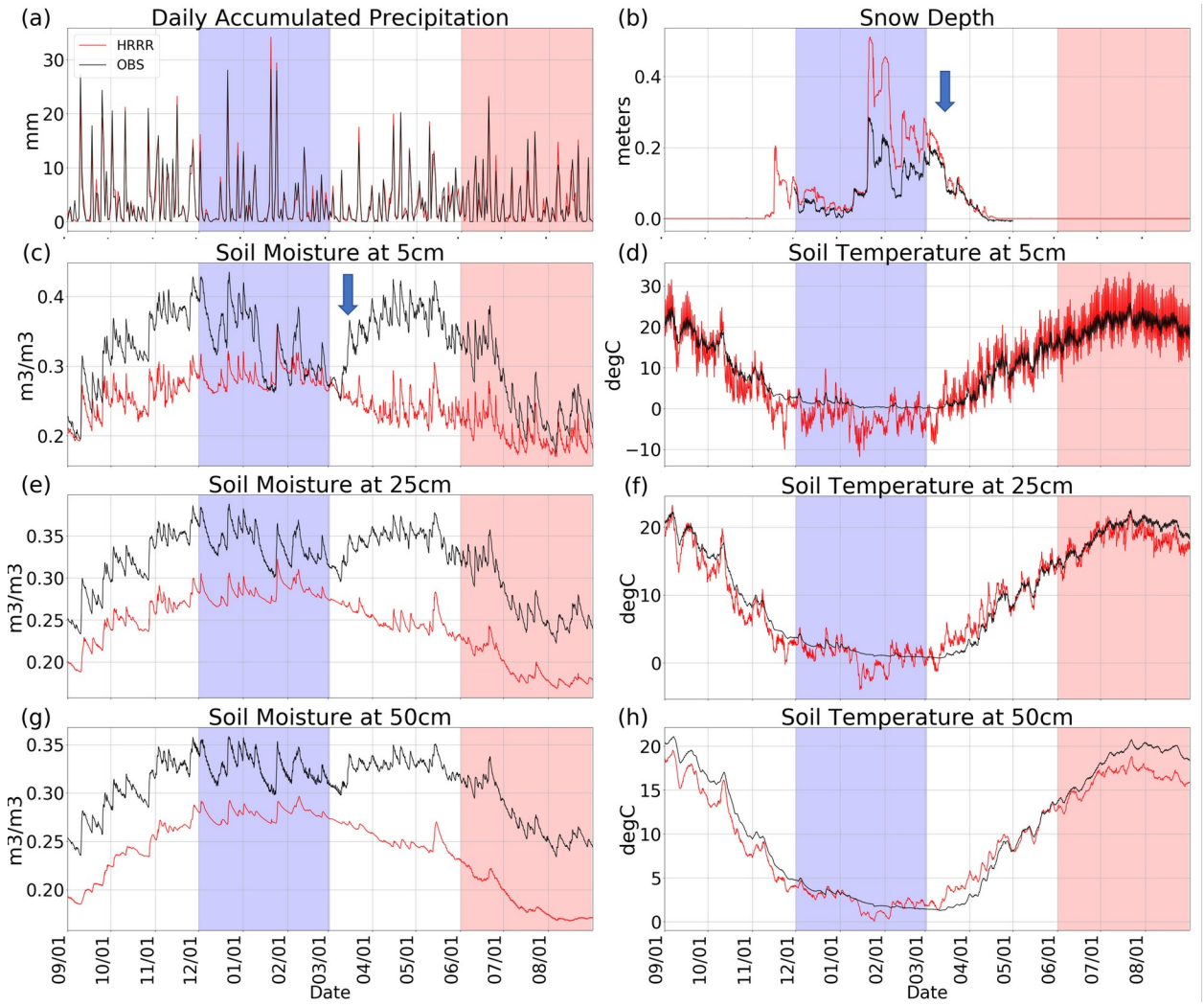

Figure 4. Time series of 126 standard sites averaged (a) daily accumulated precipitation, (b) snow depth, (c, e, g) soil moisture at 0.05 m, 0.25 m and 0.5 m; and (d, f, h) soil temperature at 0.05 m, 0.25 m, 0.5 m.

Soil moisture is an important variable among the processes that describe the land surface–atmosphere coupling. Its value reflects how rainfall is partitioned into runoff, surface storage, and infiltration components. One consequence is that soil moisture modulates the energy budget by determining the soil heat capacity, the degree of evapotransipiration, and the albedo (Seneviratne et al., 2010; Smirnova et al., 1997; Gascoin et al., 2008). Through balancing of land surface water and energy, soil moisture directly affects 2-m temperature and humidity by controlling the total energy used by latent heat flux, and further modulating surface energy partition. (Kala et al., 2016; Seneviratne et al., 2013; Mueller & Seneviratne, 2014). Soil moisture at all three levels of 0.05 m, 0.25 m, 0.5 m are closely associated with the precipitation.

The spikes of precipitation-induced soil moisture increase matches alright between model and observation (Figures 4a, 4c, 4e and 4g).

At each mesonet station, a Stevens Hydra Probe Soil Sensor measures soil moisture based on dielectric permittivity measurements. Proprietary algorithms were used to convect the signal response of the standing radio wave into the dielectric permittivity and thus the soil moisture. The soil moisture measurements are in units of water fraction by volume (m^3/m^3), which is consistent with model. The forecasted soil moisture values at 0.25 m and 0.5 m have systematic biases around 0.05 m^3/m^3 respectively. The forecasted soil moisture at 0.05 m showed few apparent biases when compared to NYSM measurements at the beginning of the evaluation period (1 Sep, 2018), but a dry bias emerged as the fall transition proceeded (Figure 4c). During the warm days of late winter to early spring, snowmelt, which is the major reason for snow depth reduction, adds water into the soil. NYSM observation shows around 20cm snow melted during early spring and in the meantime, observed soil moisture increased sharply (blue arrow in Figure 4). However, the forecasted soil moisture at 0.05 m did not respond to the snow water as indicated by the NYSM observations. This suggests that the snow melting process is poorly represented by the HRRR, either due to RUC thawing process or due to the snow water runoff.

HRRR-forecasted soil temperatures at three levels (Figures 4d, 4f and 4h) basically agree with NYSM observations. However, HRRR predicted a much larger diurnal cycle of soil temperature at the 0.05 m and 0.25 m levels than observation (Figures 4d and 4f). One possible reason is that the overall dry biases of soil moisture decreased the soil heat capacity, and led to increased amplitude of soil temperature variation. Also, the observed average soil temperature was above freezing during the cold winter months, while HRRR-forecasted soil temperature exhibited much lower temperatures, below freezing (Figure 4d). These examples illustrate potential issues in the RUC as used by the HRRR, including difficulties simulating the soil freeze-thaw processes (Viterbo et al., 1999; Ek et al., 2003). In the real world, the water in the soil will not completely freeze, but rather remain a mixture of ice and water at 0° C. However, the model unrealistically freezes the soil at depth during the cold winter. This bias in soil temperature partly explains the extreme cold bias we see earlier in 2m air temperature.

The soil moisture budget examines one avenue of how changes in the land surface may alter the water and energy balances. Precipitation and snowmelt inputs increase soil moisture through infiltration are countered by runoff and evapotranspiration outputs, as evapotranspiration releases water through plant leaves and soil (Figure 5). The comparison between HRRR change rates and NYSM observation in four seasons exhibit unique seasonal characteristics:

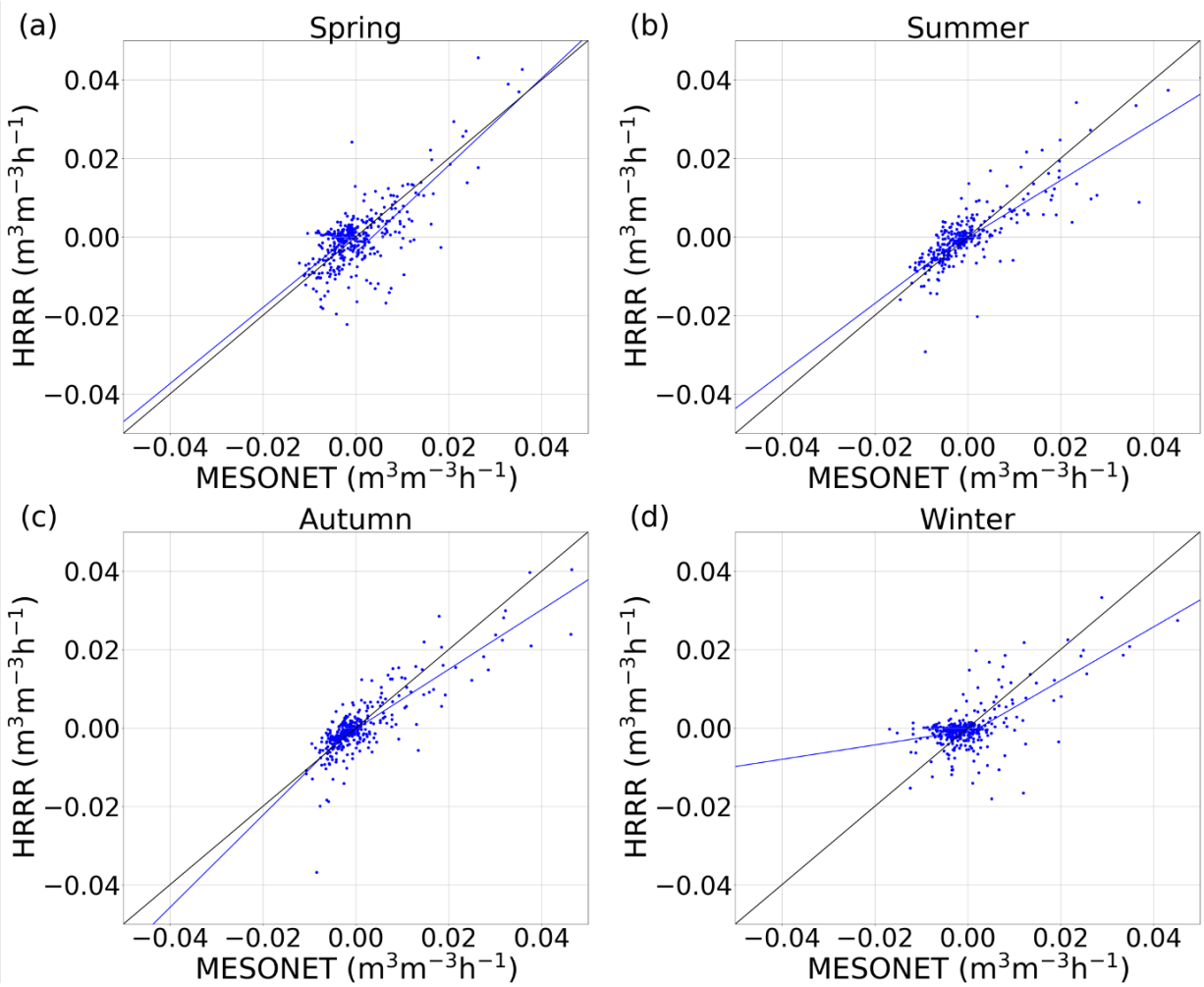

Figure 5. Mesonet observed and HRRR simulated regression fits for soil moisture differential at 0.05 m during different seasons. the growth rate and loss rate are linear fitted separately. The black lines represent the 1:1 line. The blue lines represent linear regression lines.

Table 2. Comparison of modeled with observational soil moisture rates of change under different precipitation conditions.

	loss rate			growth rate		
	r	slope	intercept	*r*	slope	intercept
Spring	0.50	0.97	0.0006	0.78	1.11	-0.0040
Summer	0.68	0.89	0.0006	0.77	0.73	-0.0001
Autumn	0.59	1.18	0.0012	0.84	0.76	-0.0002
Winter	0.19	0.18	-0.0006	0.66	0.68	-0.0016

306

307 • Spring: Snowmelt is important to soil hydrological process for soil moisture growth rate during
308 early spring season. The extreme high intercept -0.0040 $m^3m^{-3}h^{-1}$ shown in Table 2 could be
309 attributed to the misrepresentation of snow melting process. In the mean time, the loss rates of
310 soil moisture during this period are not well captured by HRRR forecasts. The loss rate
311 correlation coefficient *r* is only 0.50. The result indicates that large uncertainty still lies in the
312 soil hydrological process during spring associated with snow metling and the partition of water
313 into runoff, soil moisture and evapotranspiration.

314 • Summer: The precipitation has been underestimated in summer with the integrated bias as -
315 20.56 mm in whole summer, which lead to the underestimation of the growth rate of soil
316 moisture forecasted by HRRR in summer (Benjamin et al., 2016). The loss rate of soil moisture
317 forecasted by HRRR tended to be lower than NYSM observation, suggesting a weak
318 evapotranspiration process in HRRR RUC (Figure 5b). A combined result of the underestimation
319 of both growth and loss rates is that the overall soil moisture dry bias decreases from its
320 maximum at the beginning of summer to much less in late summer (Figure 4c). The severe
321 underestimate of evapotranspiration processes changes surface energy patition and lead to the
322 consistent warm bias observed.

323 • Autumn: The HRRR underpredicted the growth rate of soil moisture, however, overestimated
324 the loss rate during the transition season. The overestimation of loss rate in fall indicates that the
325 evapotranpiration process during autumn has been overestimated. As leaf senescence occurred in
326 New York during this period, the transpiration vanished; the vegetation ceased to withdraw
327 water from the soil. The soil moisture continued to build up and reached its annual maximun in
328 early winter. In Figure 4c, the model shows a gradual dry bias in forecasted soil moisture, with
329 almost the same level of soil moisture at the beginning (September 1st) and 0.1 m^3/m^3 bias at the
330 end of the fall (November 30th). It is likely that the vegetation phenology changes during the fall
331 and their impact on soil moisture dynamics are not well represented in HRRR RUC.

332 • Winter: The soil hydrological process is most poorly simulated in winter. The HRRR growth
333 rate of soil moisture is underpredicted, and the loss rate is largely underpredicted. During the
334 winter, precipitation can be either in liquid phase (i.e., rain) which immediately interacts with
335 soil or in solid phase (i.e., snow) accumulated for later release. The soil freezing and thawing
336 processes adds more complexity to the soil moisture dynamics. The observed HRRR biases
337 suggest the needs to further investigate the snow precipitation process, snow-pack dynamic and
338 the soil freeze cycle in the HRRR.

339 3.3 Surface energy partition

340 The land use types exert a major control on the surface energy partition. The way that the
341 model represents the partition of sensible and latent heat flux with different land use types is
342 crucial to the forecast of land surface meteorological condition and cloud formation through land
343 atmosphere feedbacks. To gain deeper insight into model performance, HRRR forecasted energy
344 partition at three major land use type sites of forest, farmland forest mosaic, and urban are
345 evaluated using the flux measurements from NYSM flux sites. Three typical flux sites (REDF,
346 VOOR, STAT, shown in Figure 1) were selected for the further analysis. We only selected the
347 sites that have the same land use type as does the 3km model land use classification. However, it

should also be noted that, for three selected flux sites, the immediate surrounding area is flat with grassland or low vegetation to meet WMO standards. To get the best representation of heat fluxes from different land use types, only the data from mid-afternoon (1800 UTC) are used. During this period, the impact of surrounding land cover on the flux measurements is most significant due to that the mixing of boundary layer is strongest at this time of the day.

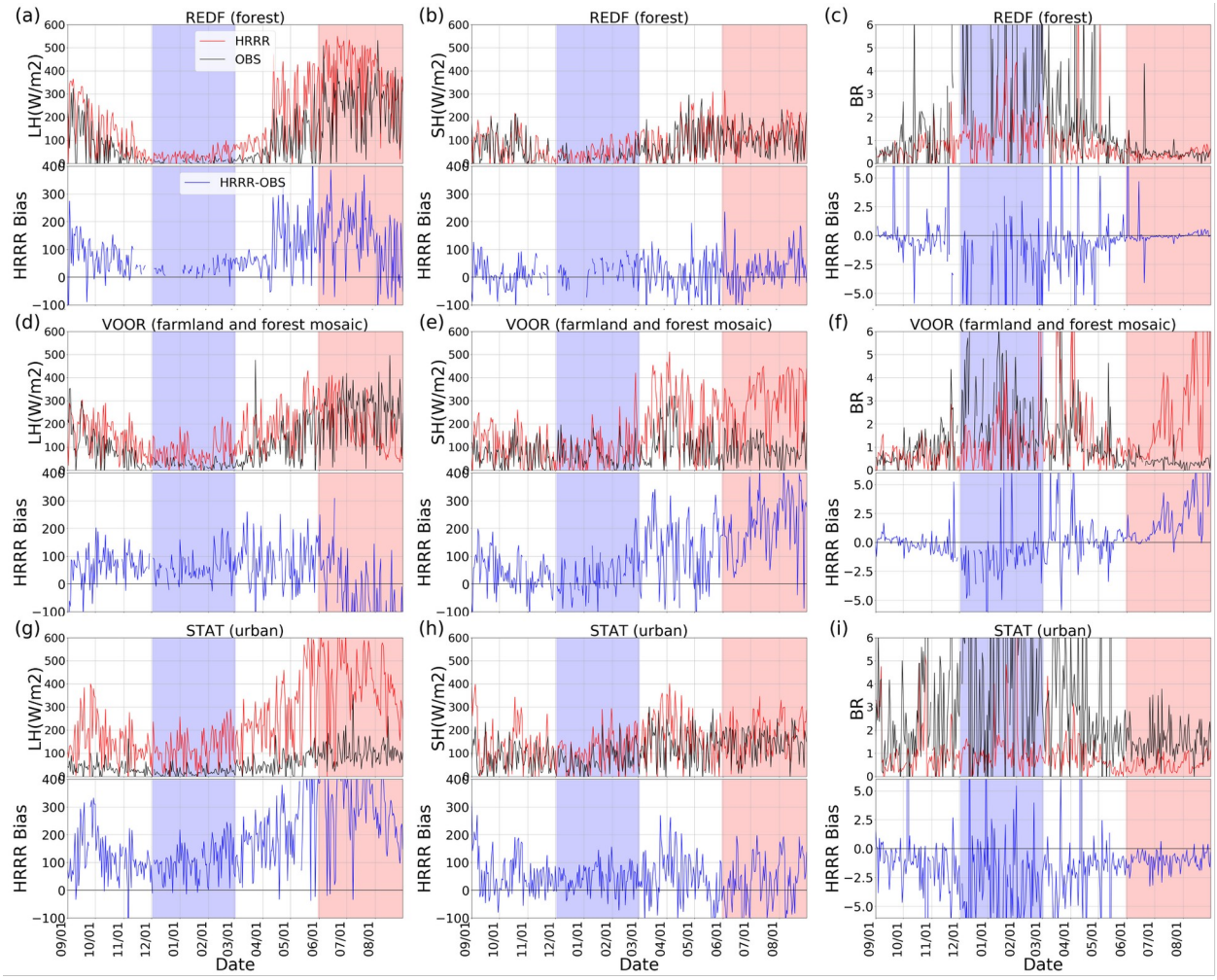

Figure 6. Time series of (a, b, c) daytime latent heat flux, sensible heat flux, Bowen ratio measured from forest flux site; (d, e, f) from farmland flux site; (g, h, i) from urban flux site

At forest sites during the warm season, the latent heat flux is overestimated, and the sensible heat flux is close to the measurements. However, considering that the observed fluxes have an estimated 100W/m^2 to 200W/m^2 energy closure imbalances (Steeneveld et al., 2011), it is possible that the sensible heat flux has been underestimated at the forest sites. HRRR underpredicted the mid-day Bowen ratio compared to NYSM observation for most of the growing season, from spring onset to leaf senescence (Figures 6a-6c). The bias in energy partition over forest sites partly explains the slight cold and wet bias over Adirondack region under clear sky shown in Figure 3a. Over the forest, the evapotranspiration process dominates

365 the latent heat flux during the growing season. The deep rooting system enables the forest to be
366 less affected by the surface soil moisture drought.

367 On the contrary, the HRRR predictions of Bowen ratio over farmland sites are generally
368 larger than the observed during the warm season. Compared to forest, farmland has a much
369 shallower root depth, which is more vulnerable to the water deficit at surface soil layers. As
370 discussed in section 3.2, soil moisture has been underestimated during the warm season. The
371 false drought in soil further lead to the underestimation of latent heat flux, while sensible heat
372 flux is overestimated around 300 W/m^2. This relatively larger biases of Bowen ratio over
373 farmland sites than those over forest sites consist with the larger warm bias of 2-m temperature
374 over farmland sites than those over forest sites (Figure 3). These biases will also contribute to
375 changing of the convection behavior of cloud, and further enlarge the surface thermodynamic
376 bias through surface cloud feedbacks.

377 During the snowmelt period, HRRR predicted more LH (Figure 6a) without significant
378 increase in soil moisture at 0.05 m level (Figure 4c). In fact, Figure 4c shows that 0.05 m soil
379 moisture in HRRR decreases steadily during this period, while the observation increases rapidly.
380 The result suggests that most melt water was evaporated into the atmosphere and did not
381 infiltrate into the soil.

382 Over the urban site, the HRRR overestimated the latent heat while underestimating the
383 Bowen ratio. The urban site equipment are located on rooftop, and that the measurements are
384 affected by artificial local heat sources.

385 The 2-m air temperature and humidity biases over New York State have quite unique
386 spatial characteristics. The biases are small over forest and largest over farmland. (see Figure 3
387 and Table 1). The vertical flux divergence of surface sensible and latent heat fluxes simulated by
388 land surface model modifies the atmosphere heat and moisture state. Correct representation of
389 surface energy partition is essential to simulation of the 2-m (screen level) and mixed layer
390 temperature and humidity. The significant overestimation of Bowen ratio and underestimation of
391 latent heat over farmland (see Figures 6d-6f) is possibly one of the most important sources of the
392 2-m temperature and humidity spatial related biases.

393 During the warm season, the underestimation/overestimation of the Bowen ratio over
394 forest/farmland sites led to the cold/warm and wet/dry biases under clear sky. The dry bias in soil
395 moisture, and underestimated evapotranspiration in the warm season partially explains the bias in
396 surface energy budget estimates. The early-spring snowmelt issue could be one of the reasons
397 that leads to the warm and dry biases during the subsequent warm season. As a consequence of
398 insufficient water infiltrating into the soil in spring, there arises a soil water deficit at the
399 beginning of summer, and this suppresses evapotranspiration and latent heat release especially
400 over regions with shallower-rooted vegetation.

401

402 3.4 Cloud radiative effects on land-atmosphere coupling biases

403 The 2-m air temperature and humidity biases over New York State are close associated
404 with observed cloud conditions (see Figure 3). Under clear sky, the biases are smallest, while
405 under the thickest cloud, the biases are largest. Possible causes from cloud radiative forcing in
406 the model should be investigated. Underestimation of low-level cloud coverage and optical
407 thickness has been identified as an important potential explanation for the systematic daytime

incoming solar radiation bias, in turn yielding a surface warm and dry bias during the warm season (Benjamin et al. 2016). Here the biases of downward shortwave radiation and maximum 2-m air temperature are investigated by classifying biases using clear sky index.

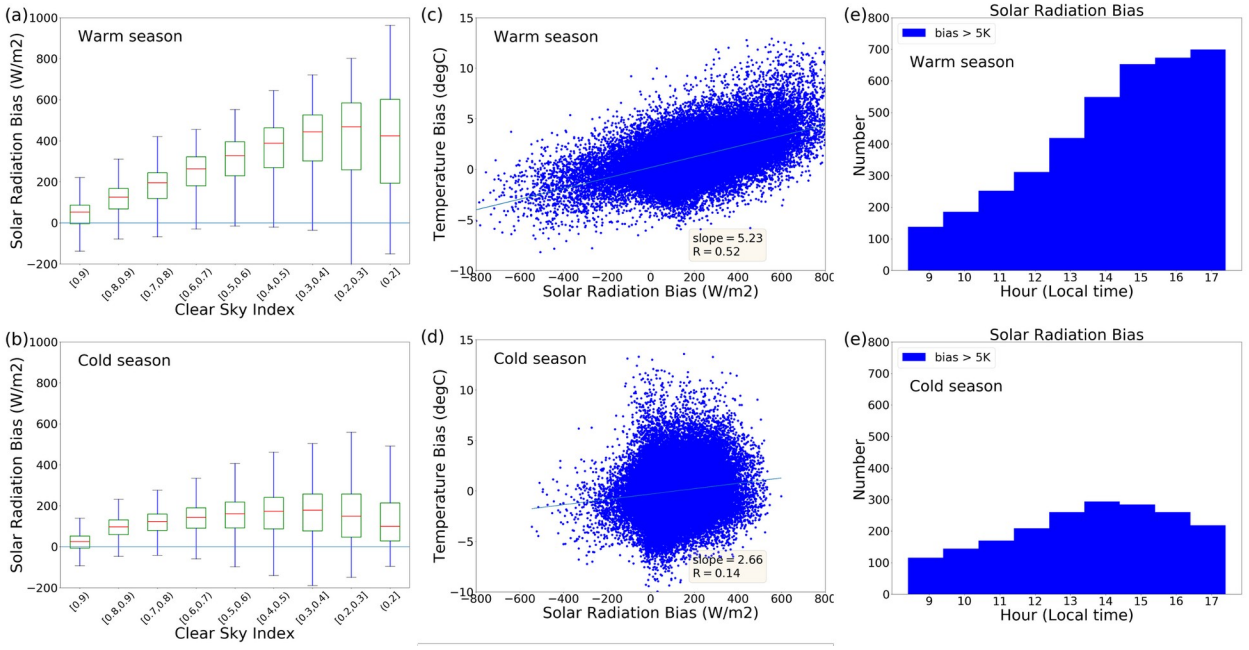

Figure 7. (a,b) Box-and-whisker plots showing the shortwave radiation bias binned by clear sky index (warm/cold season). The vertical bar represents standard error. (c,d) correlations between downward shortwave radiation bias and daily maximum temperature bias; (e, f) Number of measurements in certain hours when the temperature biases exceed 5 K. The warm season is June, July, August (JJA), and the cold season is December, January and February (DJF). Only daytime (from 9:00 to 16:00 local time) data are included in the statistics.

Figure 7a shows that during the warm season, both the mean biases and standard deviation of the shortwave radiation increases as observed clouds thicken (The clear-sky index in Figure 7 is based on station observation). In the warm season, a positive radiation bias around 100 W/m^2 when the clear sky index exceeds 0.9. The absence of aerosol direct effect in HRRR could be the reason for this positive bias under clear sky. For clear sky index < 0.2, when the sky is covered by optically thick clouds, the mean radiation bias can be as high as 400 W/m2. In contrast to previous studies that emphasized the importance of unresolved fair-weather sub-grid clouds on the surface temperature bias, our analysis indicates that largest radiation biases are associated with optically thicker clouds. During the warm season, the clouds over North Eastern United States (NEUS) can be separated into four categories: Fair weather cumulus, cumulus congestus (towering cumulus), individual cumulonimbus, and stratocumulus associated with thunderstorm and frontal passage (Houze, 1993). The GOES truecolor cloud images and synopic weather maps during this period show that the days associated with the large biases and low cloud index are generally associated with individual cumulonimbus and stratocumulus associated with thunderstorm and frontal passage. The displacement and weaker strength in deep convection might explain most of the biases in thick clouds.

During the warm season, daytime temperature bias correlates well with the shortwave radiation bias (Figure 7c) . Further analysis separates the radiation and temperature biases using the clear sky index. In both warm and cold seasons, it is clearly shown (Table 3) that the slope of the linear regression between solar radiation and temperature biases decreases as the clear sky index increases, as does the correlation coefficient r. The results suggest that when clouds are thicker, the temperatue biases are explained more by the radiation biases. This further supports the argument that the relationship between radiation bias and temperature bias is more significant with thicker clouds.

The dependence of shortwave biases on cloud is more significant in warm season than during the cold season (Figures 7a and 7b). Compared to the warm season, the cold season daytime temperature bias is much less dependent on cloud bias. When the clear sky index exceeds 0.4, the slope becomes negative, and the correlation coefficient essentially vanishes. During cold season, other process rather than shortwave radiation forcing dominates the boundary layer thermodynamic process, such as the high albedo of surface snow and longwave cloud forcing. (Betts & Beljaars, 2017). Also, due to the much thinner convective boundary layer, the surface thermodynamically-controlled boundary layer cloud fraction is lowest during cold season over the eastern United States (Freedman et al., 2001). These results suggested that other physical processes, such as the snow albedo effect and snow/soil frozen/melting process may be more important to explain the surface temperature biases (Figure 7d).

Table 3. Relationships between solar radiation biases and air temperature biases during warm and cold season. The results are classified by clear sky index (CSI). The slope has been multiplied by scale factor of 1000, and the unit of slope is °C/(W/m^2). W indicates warm season, C indicates cold season. *r* is the correlation coefficient.

CSI	[0, 0.2]	[0.2,0.3]	[0.3,0.4]	[0.4,0.5]	[0.5,0.6]	[0.6,0.7]	[0.7,0.8]	[0.8,0.9]	[0.9,1]
Slope(W)	5.79	4.43	4.00	3.65	3.18	3.50	3.03	2.92	3.22
r (W)	0.54	0.50	0.47	0.46	0.39	0.32	0.26	0.23	0.20
Slope (C)	1.74	1.53	0.45	-0.21	-0.77	-0.13	0.02	-0.22	-0.05
r (C)	0.09	0.09	0.03	-0.01	-0.04	-0.01	0.00	0.01	0.00

Figures 7e and 7f illustrates the interesting feature that extreme temperature biases larger than 5 K (assumed to be a temperature forecast error) is more frequent at 15:00 LT, typically considered to be the warmest time of day. However, another possible reason for the largest temperature biases may be associated with occasional afternoon thunderstorms, which occur around 15:00. The histogram of cold season extreme temperature biases are much flatter than during warm season, indicating that the frequency of extreme temperature bias does not correspond to the time of day as during the warm season.

Shortwave cloud radiative forcing is the dominant process that drives boundary layer development during the warm season. Since downward shortwave radiative flux is the major source of surface energy and temperature increases during daytime, it is not surprising that the 2-m temperature biases have strong dependence on radiation biases. The relationships between cloud shortwave radiative forcing and temperature biases were analyzed. Using the clear sky index as a proxy for the observed cloud radiative forcing, the results (Figure 7a) indicated that HRRR-simulated shortwave radiation biases increase as clouds thickens. Downward shortwave

radiation biases are directly linked to low cloud amount and properties. The results suggest that during warm season, the thick and overcast clouds are the main contributor to the downward shortwave radiation positive biases. The correlation coefficient of temperature vs. radiation biases increases as cloud gets thicker, indicating that they are major source of the surface temperature and radiation biases in HRRR model.

The results of this paper emphasize that understanding land surface energy partition over diverse land cover types and the important role cloud radiative forcing (especially during warm-season thick cloud conditions) is essential to reducing modelled land surface temperature and humidity biases.

4 Conclusions

In this work, we systematically evaluated the HRRR model using the New York Stae Mesonet over the complex terrain of New York State. One year of HRRR model and observation data were used in this study to investigate the biases from both diurnal and seasonal perspectives. The dense NYSM network (average distance between stations ~ 30 km) of 126 standard weather stations provides opportunities to investigate the impact of spatial heterogeneity on the land-atmosphere-cloud interaction as a coupled system.

Surface meterological fields were examined by separating the daily maximum and minimum temperature. In the warm season, there are consistent warm and dry biases at 2 meter, with a relatively small standard deviation. Cold season biases show a much larger standard deviation but smaller mean biases. Furthermore, extreme cold biases exist in the nighttime in February, with large daytime wet biases in March.

Soil hydrological processes strongly control surface energy balance and fluxes, which are the most sensitive processes in the land surface model to the atmospheric model (Santanello et al., 2019). Through the whole year, soil moisture at all measured vertical levels (0.05, 0.25 and 0.5 m) are largely underestimated, contributing to the dry and warm biases during the warm season. Also, this soil moisture underestimation reduces the soil heat capacity, causing the overestimation of soil temperature diurnal amplitude. During the cold season, the abnormal soil temperature below freezing when the observational soil temperature is close to 0°C is the possible reason for the extreme cold temperature biases during winter. Lacking a comprehensive representation of soil freezing-thawing processes, the model failed to predict a soil temperature barrier at the freezing point.

Contributions of evapotranspiration and precipiatation to soil hydrological processes from seasonal perspective were analyzed. Results show that during spring, the snow melting process controls the bias in soil moisture growth rate. During summer, the soil moisture growth rate is underestimated due to the forecast shortfall in summer thunderstorm development, this bias is compensated by the underestimate of evapotranspiration. The result is that the soil moisture dry bias decreases from its maximum at the beginning of summer to much less in late summer (Figure 4c). In fall, the model underpredicts the precipitation brought by tropical cyclones. In the meantime, evapotranspiration rate has been overestimated due to incorrect representation of seasonal transition when the leaves fall. The combined effect is a negative soil moisture of about 0.1 m^3/m^3 at the end of fall season. Winter biases mostly come from snow melting and soil freezing/thawing processes.

The dry bias in soil moisture content that appears during snow melt season is the main source for the warm season soil moisture underestimation. The soil dries out in the model while the soil is moistened by melting snow in the observations. The water stress in the model soil hydrological processes plays an important role in the energy partition in the following summer season where the water stressed soil will suppress the evapotranspiration and increase the Bowen ratio especially for shallow rooted vegetation, leading to the surface thermodynamic bias in the seasonal scales. These processes are amplified by the positive feedback loop between dry soil, reduced clouds, and warm temperatures. The positive feedback loop is most significant in warm season when the land surface atmosphere cloud coupling is strongest. This result presents a specific avenue for future model improvement: studying and improving the representation of snow melt and infiltration processes in the early spring.

Low-level clouds are recognized as one of the most important sources of the surface incident solar radiation and temperature biases. Complementing earlier analyses of the impact of sub-pixel cloud, we further explored the cloud effect by classifying cloud optical properties using clear sky index. We found that the most optically thick clouds (generally associated with frontal system and thunderstorms) yielded the largest biases in solar radiation, the main contributor to the surface warm bias during the warm season. This finding emphasized the importance of further investigation of these clouds in the model.

The present work identifies HRRR model biases from the land-atmosphere coupling perspective. Surface energy partition introduced by different land surface properties and cloud radiative forcing are two main sources of warm season 2-m temperature and humidity biases. As an integrated system, biases of each feedback elements in land-atmosphere-cloud interactions can easily spread into the whole system and further increase the overall bias and reduce the forecast accuracy. For the future application of the HRRR model to forecast the alternate energy potential as well as for severe weather forecasting, our work identifies possible mechanisms responsible for the biases in the land surface processes, such as: soil hydrological, vegetation phenology. However, the improvement of the land surface model is still challenging and requires better understanding of the physical processes as well as more complicated observation network and data assimilation techniques.

Acknowledgement

This work was supported by the US Department of Energy Solar Energy Technology Office (SETO), Advancing the WRF-Solar Model to Improve Solar Irradiance Forecast in Cloudy Environments Program under contract number 82961. The data from New York State Mesonet is available under: http://www.nysmesonet.org/weather/requestdata. The HRRR model simulations are available under: https://www.nco.ncep.noaa.gov/pmb/products/hrrr/.

References

Benjamin, S. G., Weygandt, S. S., Brown, J. M., Hu, M., Alexander, C. R., Smirnova, T. G., et al. (2016), A North American hourly assimilation and model forecast cycle: The rapid refresh. *Monthly Weather Review*, *144*(4), 1669–1694. doi:10.1175/MWR-D-15-0242.1.

Betts, A. K., & Silva Dias, M. A. F. (2010), Progress in understanding land-surface-atmosphere coupling from LBA research. *Journal of Advances in Modeling Earth Systems*, *2*, 6, doi:

10.3894/JAMES.2010.2.6.

Betts, A. K., & Beljaars A. C. M. (2017), Analysis of near-surface biases in ERA-Interim over the Canadian Prairies. *Journal of Advances in Modeling Earth Systems*, *9*, 2158–2173. doi:10.1002/2017MS001025.

Brotzge, J. A., Wang, J., Thorncroft, C. D., Joseph, E., Bain, N., Bassill, N., et al. (2020), Technical overview of the New York State Mesonet Standard Network. *Journal of Atmospheric and Oceanic Technology*, 1–48, 1–48. doi:10.1175/JTECH-D-19-0220.1

Bytheway, J. L., Kummerrow, C. D., & Alexander, C. R. (2017), A Features-Based Assessment of the Evolution of Warm Season Precipitation Forecasts from the HRRR Model over Three Years of Development. *Weather and Forecasting*, *32*(5), 1841–1856. doi:10.1175/WAF-D-17-0050.1.

Covert, J. M. (2019), Design and Implementation of the New York State Mesonet Flux Tower Network. State University of New York at Albany, 99 pp. https://search.proquest.com/dissertations-theses/design-implementation-new-york-state-mesonet-flux/docview/2232975746/se-2?accountid=14166.

Ek, M. B., Mitchell, K. E., Lin, Y., Rogers, E., Grunmann, P., Koren, V., Gayno, G., & Tarpley, J. D. (2003), Implementation of Noah land surface model advances in the National Centers for Environmental Prediction operational mesoscale Eta model. *Journal of Geophysical Research*, *108*(D22), 8851. doi:10.1029/2002JD003296.

Eltahir, E. A. B. (1998), A soil moisture–rainfall feedback mechanism 1. Theory and observations. *Water Resources Research*, *4*(34), 765–776.

Fitzjarrald, D. R., Acevedo, O. C., & Moore, K. E. (2001), Climatic consequences of leaf presence in the eastern United States. *Journal of Climate*, *14*, 598–614.

Freedman, J. M., Fitzjarrald, D. R., Moore, K. E., & Sakai, R. K. (2001), Boundary Layer Clouds and Vegetation-Atmosphere Feedbacks. *Journal of Climate*, *14*, 180–197.

Freedman, J. M., & Fitzjarrald, D. R. (2017), Mechanisms Responsible for the Observed Complex Structure in a Convective Boundary Layer Over the Hudson Valley. *Boundary-Layer Meteorology*, *164*, 89–106. doi: 10.1007/s10546-017-0241-6.

Garc´ıa-D´ıez, M., Fern´andez, J., Fita, L., & Yag¨ue, C. (2013), Seasonal dependence ofWRFmodel biases and sensitivity to PBL schemes over Europe. *Quarterly Journal of the Royal Meteorological Society*, *139*(671), 501–514. doi:10.1002/qj.1976.

Gascoin, S., Ducharne, A., Ribstein, P., Perroy, E., & Wagnon P. (2009), Sensitivity of bare soil albedo to surface soil moisture on the moraine of the Zongo glacier (Bolivia). *Geophysical Research Letters*, *36*, L02405. doi:10.1029/ 2008GL036377.

Griffin, S. M., Otkin, J. A., Rozoff, C. M., Sieglaff, J. M., Cronce, L. M., Alexander, C. R.,

Jensen, T. L., & Wolff, J. K. (2017), Seasonal analysis of cloud objects in the High-Resolution Rapid Refresh (HRRR) model using object-based verification. *Journal of Applied Meteorology and Climatolog*, *56*, 2317–2334. doi: 10.1175/JAMC-D-17-0004.1.

Houze, R. A.Jr. (1993), Cloud Dynamics, 5 pp., Academic, San Diego, Calif.

Iacono, M. J., Delamere, J. S., Mlawer, E. J., Shephard, M. W., Clough, S. A., & Collins, W. D. (2008), Radiative forcing by long–lived greenhouse gases: Calculations with the AER radiative transfer models. *Journal of Geophysical Research: Atmospheres*, *113*, D13103. doi:10.1029/2008JD009944 .

James, E. P., Benjamin, S. G., & Marquis, M. (2017), A unified high-resolution wind and solar dataset from a rapidly updating numerical weather prediction model. *Renewable Energy*, *102*(Part B), 390–405. doi:10.1016/j.renene.2016.10.059.

James, E., Ahmadov, R., & Grell, G. A. (2018), Realtime Wildfire Smoke Prediction in the United States: the HRRR-Smoke Model. *EGU General Assembly Conference Abstracts*, *20*, p. 19526.

Kala, J., De Kauwe, M. G., Pitman, A. J., Medlyn, B. E., Wang, Y.-P., Lorenz, R., & Perkins-Kirkpatrick, S. E. (2016), Impact of the representation of stomatal conductance on model projections of heatwave intensity. *Nature Science Report*, *6*, 23418. doi:10.1038/srep23418.

Katona, B., Markowski, P., Alexander, C., & Benjamin, S., (2016), The influence of topography on convective storm environments in the eastern United States as deduced from the HRRR. *Weather and Forecasting*, *31*(5), 1481–1490. http://dx.doi.org/10.1175/WAF-D-16- 0038.1.

Koster, R. D., et al. (2004), Regions of strong coupling between soil moisture and precipitation. *Science*, *305*, 1138–1140. doi:10.1126/ science.1100217.

Koster, R. D., et al. (2006), GLACE: The global land-atmosphere coupling experiment. Part I: Overview. *Journal of Hydrometeorology*, *7*(4), 590–610.

Lee, T. R., Buban, M., Turner, D. D., Meyers, T. P., & Baker, B. (2019), Evaluation of the High-Resolution Rapid Refresh (HRRR) Model Using Near-Surface Meteorological and Flux Observations from Northern Alabama. *Weather and Forecasting*, *34*, 635–663. doi: 10.1175/WAF-D-18-0184.1.

Min, Q. L., & Harrison, L. C. (1996), Cloud properties derived from surface MFRSR measurements and comparison with GOES results at the ARM SGP site, *Geophysical Research Letters*, *23*, 1641.

Mueller, B., & Seneviratne, S. I. (2014), Systematic land climate and evapotranspiration biases in CMIP5 simulations. *Geophysical Research Letters*, *41*, 128–134. doi:10.1002/2013GL058055.

Olson, J. B., Kenyon, J. S., Angevine, W. M., Brown, J. M., Pagowski, M., & Sušelj, K. (2019), A Description of the MYNN-EDMF Scheme and the Coupling to Other Components in WRF–

ARW. *NOAA Technical Memorandum OAR GSD*, *61*, pp. 37. doi:10.25923/n9wm-be49.

Peters, J. M., Nielsen, E. R., Parker, M. D., Hitchcock, S. M., & Schumacher, R. S. (2017), The Impact of Low-Level Moisture Errors on Model Forecasts of an MCS Observed during PECAN. *Monthly Weather Review*, *145*(9), 3599–3624. doi: 10.1175/MWR-D-16-0296.1.

Pichugina, Y. L., et al., (2017), Assessment of NWP forecast models in simulating offshore winds through the lower boundary layer by measurements from a ship-based scanning Doppler lidar. *Monthly Weather Review*, *145*(10), 4277–4301. doi: 10.1175/MWR-D-16-0442.1.

Pleim, J., & Ran, L. (2011), Surface flux modeling for air quality applications. *Atmosphere*, *2*(3), 271–302. doi:10.3390/atmos2030271.

Robledo, L. & Soler, A. (2000), Luminous efficacy of global solar radiation for clear skies. *Energy Conversion and Management*, *41*(2000), 1769–1779.

Schar, C., Luthi, D., Beyerle, U., & Heise, E. (1999), The soil-precipitation feedback: A process study with a regional climate model. *Journal of Climate*, *12*(3), 722–741.

Seneviratne, S. I., Corti, T., Davin, E. L., Hirschi, M., Jaeger, E. B., Lehner, I. et al . (2010), Inverstigating soil moisture−climate interactions in a changing climate: a review. *Earth-Science Reviews*, *99*(3-4), 125–161. doi:10.1016/j.earscirev.2010.02.004.

Seneviratne, S. I., et al. (2013), Impact of soil moisture–climate feedbacks on CMIP5 projections: First results from the GLACE-CMIP5 experiment. *Geophysical Research Letters*, *40*, 5212–5217. doi: 10.1002/grl.50956.

Smirnova, T. G., Brown, J. M., & Benjamin, S. G. (1997), Performance of Different Soil Model Configurations in Simulating Ground Surface Temperature and Surface Fluxes. *Monthly Weather Review*, *125*(8), 1870–1884. doi: 10.1175/1520-0493(1997)125<1870:PODSMC>2.0.CO;2.

Smirnova, T. G., Brown, J. M., Benjamin, S. G., & Kim, D. (2000). Parameterization of cold−season processes in the MAPS land−surface scheme. ***Journal of Geophysical Research: Atmospheres***, 105, 4077– 4086. doi: 10.1029/1999JD901047Smirnova, T. G., Brown, J. M., Benjamin, S. G., & Kenyon, J. S. (2016), Modifications to the Rapid Update Cycle Land Surface Model (RUC LSM) Available in the Weather Research and Forecasting (WRF) Model. *Monthly Weather Review*, *144*(5), 1851–1865. doi: 10.1175/MWR-D-15-0198.1

Steeneveld, G. J., Tolk, L. F., Moene, A. F., Hartogensis, O. K., Peters, W.,& Holtslag, A. A. M. (2011), Confronting the WRF and RAMS mesoscale models with innovative observations in the Netherlands: Evaluating the boundary layer heat budget. *Journal of Geophysical Research: Atmospheres*, *116*, D23114. doi:10.1029/2011JD016303.

Stull, R. B., (1988), An Introduction to Boundary Layer Meteorology. Netherlands: Springer.doi: 10.1007/978−94−009−3027−8_7.

Sun, X., Holmes, H. A., Osibanjo, O. O., Sun, Y., Cesunica E., & Ivey, C. E. (2017), Evaluation

of Surface Fluxes in the WRF Model: Case Study for Farmland in Rolling Terrain. *Atmosphere*, *8*(10), 197. doi:10.3390/atmos8100197.

Taylor, C. M., Richard, D. A. M., Guichard, F., Harris, P. P. & Dorigo, W. A. (2012), Afternoon rain more likely over drier soils. *Nature*, *489*, 423–426. doi:10.1038/nature11377

Thompson, G., & Eidhammer, T. (2014), A study of aerosol impacts on clouds and precipitation development in a large winter cyclone. *Journal of the Atmospheric Sciences*, *71*(10), 3636–3658. doi:10.1175/ JAS-D-13-0305.1.

Wagner, T., P. Klein, & Turner, D. (2019), A new generation of ground-based mobile platforms for active and passive profiling of the boundary layer. *Bulletin of the American Meteorological Society*, *100*(1), 137–153. doi: 10.1175/BAMS-D-17-0165.1.

Williams, I. N., Lu, Y., Kueppers, L. M., Riley, W. J., Biraud, S. C., Bagley, J. E. & Torn, M. S. (2016), Land-atmosphere coupling and climate prediction over the U.S. Southern Great Plains. *Journal of Geophysical Research: Atmospheres*, *121*, 12125–12144. doi:10.1002/2016JD025223.

Yang, J., & Min, Q. (2018), Retrieval of atmospheric profiles in the New York State Mesonet using one-dimensional variational algorithm. *Journal of Geophysical Research: Atmospheres*, *123*, 7563–7575. doi: 10.1029/ 2018JD028272.

Min, Q. L., and L. C. Harrison (1996), Cloud properties derived from surface MFRSR measurements and comparison with GOES results at the ARM SGP site, *Geophys. Res. Lett.*, *23*, 1641.

Viterbo, P., Beljaars, A., Mahfouf, J. F., & Teixeira, J. (1999), The representation of soil moisture freezing and its impact on the stable boundary layer. *Quarterly Journal of the Royal Meteorological Society*, *125*(559), 2401–2426. doi: 10.1002/qj.49712555904.